Proceedings of the 12th International Conference of Control Systems, and Robotics (CDSR 2025)
July 13, 2025 - July 15, 2025 | Imperial College London Conference Center, London, United Kingdom
Paper No. 147
DOI: 10.11159/cdsr25.147

A New Type of Non-contact Integrated Sensor with Vibration Displacement and Velocity for Active Magnetic Bearing Rotor Systems

Wengheng Li[1], Changsheng Zhu[1], Tianhao Zhou[1]
[1]Zhejiang University
Zheda Road No.38, Zhejiang Province, China
whengli@zju.edu.cn; zhu_zhang@zju.edu.cn; zhouth_419@zju.edu.cn

Abstract **-** In existing displacement-controlled active electromagnetic bearing (AMB) systems, differential blocks of PID or phase lead compensators are typically used to generate damping and stabilise the rotor system. However, the noise in the displacement signal is subsequently amplified, leaving the debuggers struggling with the trade-off between damping and noise. In this paper, we propose a method to measure the vibration velocity of the rotor using the law of electromagnetic induction, and a design of an integrated sensor. The sensor mixes the velocity measurement magnetic circuit into the inductive displacement sensor, which allows for simultaneous measurement of vibration displacement and velocity in a single structure, avoiding extra axial space. Experimental results show that the noise level in the control current is significantly reduced by replacing the differential blocks of the PID with the vibration velocity feedback. The controller produces Greater damping can be produced by the controller and the vibration near the bending critical speeds of the AMB flexible rotor system can be effectively controlled.

Keywords**:** active magnetic bearing, vibration measurement, critical speed, vibration suppression

1. Introduction

Active magnetic bearings (AMBs) represent a superior alternative to conventional mechanical bearings, owing to their contact-free operation, reduced power losses, elimination of the need for lubrication, and the ability to control the vibrations of rotor systems [1,2]. In the past, the rotor vibration measurement was mainly based on the displacement sensors. To stabilize the AMBs system and suppress the vibrations in different critical speed regions, the controller must provide sufficient damping for rotor systems. Typically, it is realized by derivative blocks and phase lead filters [3,4] based on the displacements. Nevertheless, the noise amplification is unavoidable, which leaves the debuggers struggling with the trade-off between damping and noise. If the vibration velocity signal is available for direct feedback, the control of AMBs systems will be much easier. The existing non-contact velocity sensors are designed based on the Doppler effect [5-7], which is complex and not suitable for AMBs systems with limited axial space. More research is needed for non-contact vibration velocity measurement in the AMBs systems.

In this paper, an integrated sensor that measuring the vibration displacement and vibration velocity in a single structure is designed. The vibration displacement is measured by the inductive coils and the vibration velocity is measured by Faraday's law of electromagnetic induction. By introducing the vibration velocity signal directly into the feedback system instead of using the differential blocks of the PID controller, a significant reduction in the noise level of the system can be achieved. Damping of the rotor system can also be increased by velocity feedback to reduce vibration near the critical speeds.

2. Non-contact integrated sensor for vibration displacement and velocity

The basic structure of the proposed non-contact integrated sensor for vibration displacement and velocity is shown in Fig. 1. It consists of C-shaped stator cores, Y-shaped stator cores, permanent magnets (PMs), displacement coils A and B, velocity coils A and B, stator supporting and other parts. The C-shaped iron core, displacement coils and rotor form a C-shaped displacement measuring structure. The C-shaped core, PM, Y-shaped core and rotor form an E-shaped structure for vibration velocity measurement. Differential measurement is realized by mounting another sensor stator symmetrically in the same measurement direction.

2.1. Vibration displacement measurement

The basic principle of inductive vibration displacement sensor is based on the change in inductance due to the change in air gap reluctance of a closed magnetic circuit. The closed magnetic circuit is shown in Fig. 1.

The stator reluctance is

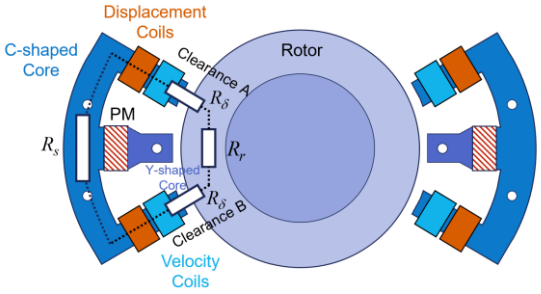

Fig. 1: Structure diagram of integrated sensor stator.

$$R_s = \frac{L_s}{\mu_0 \mu_s A_s}, \tag{1}$$

where L_s is magnetic circuit length of the stator core, μ_0 is vacuum permeability, μ_s is relative permeability of core material, and A_s is cross-sectional area of stator core perpendicular to the direction of the magnetic circuit.

The rotor reluctance is

$$R_r = \frac{L_r}{\mu_0 \mu_r A_r}, \tag{2}$$

where L_r is length of the rotor magnetic circuit, μ_r is relative permeability of the rotor material, and A_r is cross-sectional area within the rotor perpendicular to the direction of the magnetic circuit.

The air gap magnetoresistance is

$$R_\delta = \frac{\delta}{\mu_0 A_\delta}, \tag{3}$$

where δ is the length of the air gap. A_δ is equivalent area of the air gap. Magnetic leakage is a key factor in nonlinearity. Taking a second order polynomial to consider magnetic leakage [8], the equivalent area of the air gap is

$$A_\delta = \left[a + \frac{0.307}{\pi}\left(k_{\delta 11}\delta + k_{\delta 12}\delta^2\right)\right] \cdot \left[b + \frac{0.307}{\pi}\left(k_{\delta 21}\delta + k_{\delta 22}\delta^2\right)\right], \tag{4}$$

where a and b are side lengths of the air gap cross-sectional area, and $k_{\delta 1,2}$ is magnetic leakage coefficient. The value of the leakage coefficient $k_{\delta 1}$ can range from 1 to 3, and the value of the leakage coefficient $k_{\delta 2}$ can range from 10^3 to 10^4. When a or b is in the same order of magnitude as the air gap length, the corresponding leakage coefficients should take larger values. The magnetic leakage between the C- and Y- shaped cores is neglected because of the large reluctance of the PMs.

The coil self-inductance is calculated from the total reluctance of the closed loop. The coils on the same side are connected in series. Assuming the rotor displacement is $\Delta\delta$, the air gap length becomes δ-$\Delta\delta$ for coil 1 and δ+$\Delta\delta$ for coil 2. The air gap reluctance corresponding to coils 1 and 2 are calculated according to the air gap reluctance equations as $R_{\delta 1}$ and $R_{\delta 2}$, respectively.

The self-inductance of coil 1 and 2 is calculated as:

$$L_1 = \frac{N_1^2}{R_s + R_r + 2R_{\delta 1}}, L_2 = \frac{N_2^2}{R_s + R_r + 2R_{\delta 2}}, \tag{5}$$

where N_1 and N_2 are the number of turns of coils 1 and 2 respectively.

The sensor coils are excited by a sinusoidal excitation source. The two sets of coils for differential measurement are connected in series. Output signal is set at the centre of the series connection. Because thin silicon steel sheets were used, the eddy current effect is neglected. Let the amplitude of the sinusoidal excitation source be U_s and the angular velocity be ω, then the output voltage U_O is:

$$\dot{U}_o = \frac{R_{L2} + j\omega L_2}{R_{L1} + j\omega L_1 + R_{L2} + j\omega L_2}\dot{U}_s, \tag{6}$$

where $R_{L1,2}$ are resistance of coils 1 and 2, respectively. Considering different $\Delta\delta$, the displacement-voltage curves of inductive displacement sensor can be calculated.

2.2. Vibration velocity measurement

The non-contact approach to vibration velocity measurement is based on the principle of electromagnetic induction by flux changes in a closed magnetic circuit resulting from variations in air gap reluctance. As is shown in Fig. 9 (a), the equivalent magnetic circuit of the PM corresponds to a constant magnetic potential in the magnetic circuit, which is connected in series with a reluctance. The magnetic circuit includes four parts: the C- and Y-shaped core reluctance, air-gap A/B reluctance, rotor reluctance, and leakage reluctance between C- and Y- shaped core.

The PM's equivalent magnetic potential F_c is

$$F_c = H_c h_m, \tag{7}$$

where H_c, h_m are coercive force and thickness of the PM, respectively.

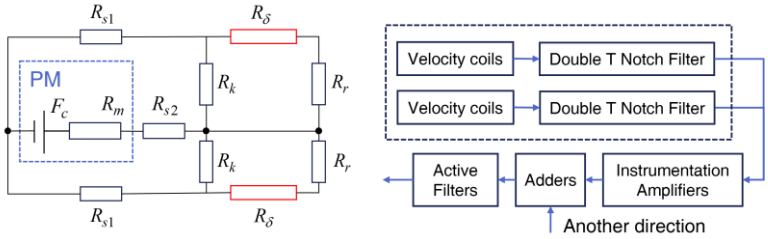

(a) The magnetic circuit of vibration velocity measurement. (b) The processing of velocity signals.
Fig. 2: The diagram of vibration velocity measurement.

The PM's reluctance R_m is

$$R_m = \frac{h_m}{\mu_0 \mu_m A_m}, \tag{8}$$

where A_m, μ_m are cross-sectional area and permeability of the PM, respectively. μ_0 is vacuum permeability. R_k is due to the leakage of magnetism between the C- and the Y-shaped core, which can be calculated by the same formula as that for the air gap reluctance. Since the two cores are not parallel, the air gap length can be chosen as an average length.

To simplify the calculation, it is assumed that the two air gaps are symmetric. The rotor reluctance R_r is neglected. The magnetic flux Φ_m is calculated by the following equation

$$\Phi_m = F_c \left[\frac{1}{2} \left(R_{s1} + \frac{R_k R_\delta}{R_k + R_\delta} \right) + R_m \right]^{-1}. \tag{9}$$

Vibration of rotor induces a change in the air gap reluctance. Let D denote the amplitude of the vibration and f represent its frequency, then

$$R_\delta = \frac{\delta + D \sin(2\pi f \cdot t)}{\mu_0 A_\delta}. \tag{10}$$

Taking the derivative of Eq. (17) yields:

$$\frac{d\Phi_m}{dt} = F_c \left[\frac{1}{2} \left(R_{s1} + \frac{R_k R_\delta}{R_k + R_\delta} \right) + R_m \right]^{-2} \cdot \frac{1}{2} \frac{R_k^2 - R_\delta^2}{(R_k + R_\delta)^2} \cdot \frac{dR_\delta}{dt}. \tag{11}$$

The denominator of Eq. (19) contains variable t. Since the vibrations are much smaller than the air gap length in general, i.e., $\delta >> D_r$, the sine equation in R_δ related to t is neglected. Thus, according to the sensitivity requirement E_r of the single coil, the number of coils turns N_c can be calculated as

$$N_c = E \Big/ \frac{d\Phi_m}{dt}. \tag{12}$$

The processing of vibration velocity signals is relatively easier, as is shown in Fig. 9 (b). The velocity coils are connected and initially filtered through a double-T trap filter. This filter aims to attenuate the interference of the excitation signal due to the asymmetry of the coil parameters. The center frequency of the trap filter is the same as the excitation signal of

displacement measurement. Then, the induced electromotive force obtained from the induction coil passes through the instrumentation amplifiers, adders, and active filters. The interference from external ground access can be avoided by using isolation amplifiers. Finally, the velocity signal containing less noise, i.e., with high signal-to-noise ratio (SNR) can be obtained.

3. Experimental validation

In order to validate our designed integrated sensors, two sets of sensors and corresponding preamplifiers were fabricated. The stator is shown in a of Fig. 3. From the figure, we can see that we fabricated four radial directions for differential measurements in the x and y directions. A PM is mounted in each direction. 4 coils were wound for each stator, including 2 displacement measurement coils and 2 velocity measurement coils. They are fixed to a PCB board by screws. The sensor preamplifier we designed is shown in Fig. b. It has two layers, the first layer is the displacement signal processing circuit, and the second layer is for the velocity signal.

The basic design parameters of the proposed integrated sensor are shown in Table 1. Note that the thickness of PM is chosen to be 4 mm. With an air gap of 1.2 mm, the silicon steel sheet maintains an average magnetic flux intensity of about 0.8 T, ensuring it stay away from saturation.

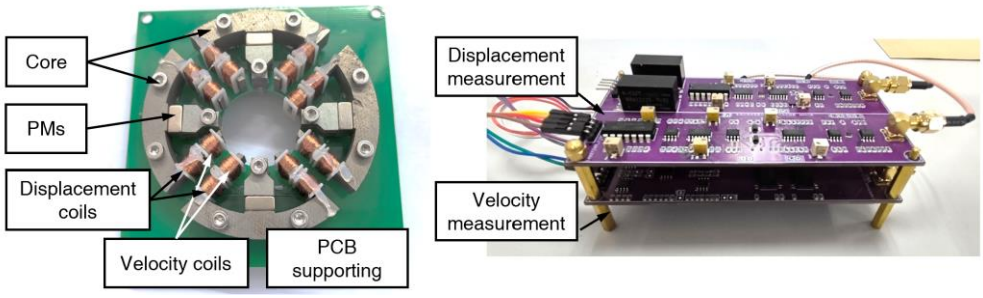

(a) The stator of the proposed integrated sensor. (b) The circuits of pre-amplifier.
Fig. 3: Photos of the designed integrated sensor.

Table 1: Basic design parameters of the integrated sensor.

Parameters	Value	Parameters	Value
Design air gap length	1.2 mm	Axial size of the sensor	25 mm
Applicable rotor diameter	25 mm	Length of core	10 mm
Output voltage range of DM	0-10 V	Material of core	Silicon steel sheets
Output voltage range of VM	-10-10 V	Coil wire diameter	0.08 mm
Stator outer diameter	78 mm	Number of turns	220
Excitation frequency	30 kHz	Thickness of PM	4 mm
PM type	NdFeB	Sensitivity of single coil	2.5 mV/mm/s

3.1. Experiments of velocity measurement and noise attenuation

As is shown in Fig. 4, the validation experiments of the integrated sensor are carried out on an AMBs multi-disk flexible rotor system test setup. It mainly consists of an 18 kg flexible rotor, two radial AMBs, drive motor and AMB's digital control system. The maximum rotational speed of the setup is 15,000 r/min. The integrated sensors developed above are installed in both AMBs, as is shown in Fig. 4 (b) and (c). The first four orders of critical speeds of the rotors are 1,800, 2,700, 7,200, 11,000 r/min respectively.

The sinusoidal excitation current of 100 Hz is added to the AMBs when the rotor is in the steady state. Fig. 5 shows the curves of displacement and velocity measurement voltages in the preamplifier. The vibration velocity signal is 90 degrees ahead of the vibration displacement signal, which contains much less noise. The sensitivity of the vibration velocity measurement can be calculated to be 92.3 mV.s/mm.

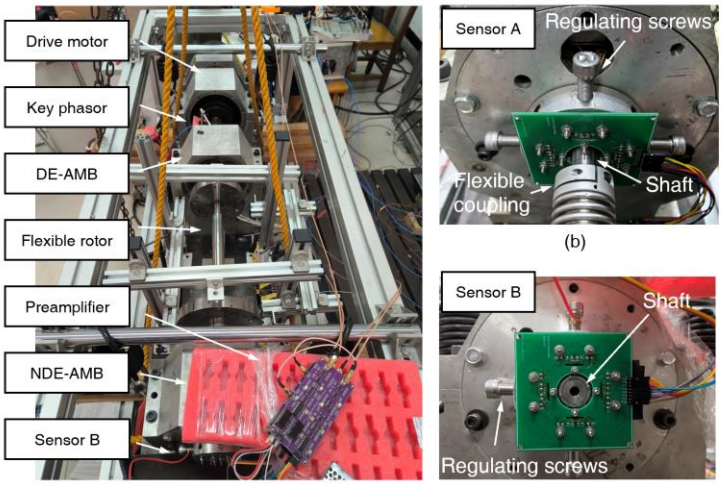

Fig.4: Photos of the test setup. (a) AMBs multi-disk flexible rotor test setup. (b) Figure of sensor A. (c) Figure of sensor B.

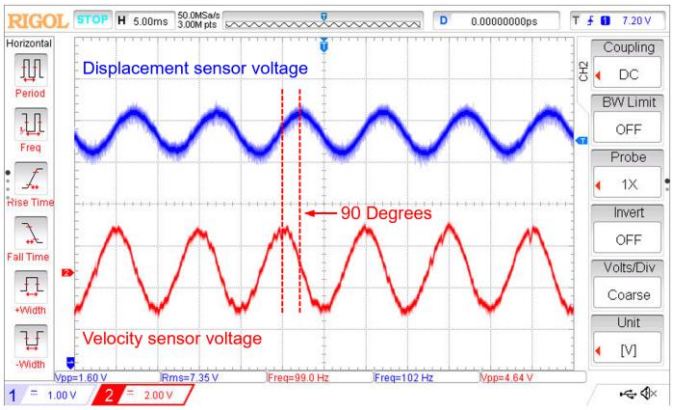

Fig. 5: Waveforms of displacement and velocity signals.

The vibration velocity signal can be fed back directly and replace the derivative block of the conventional PID controller based on the vibration displacement. Taking the Y direction of AMB-A as an example, the displacement signals and control current signals of PID, PID + velocity feedback (VF), and PI + VF tests are shown in Fig. 6.

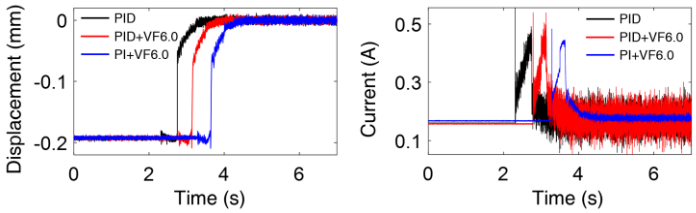

Fig. 6: Left: rotor displacement of levitation tests. Right: control currents of levitation tests.

According to previous experience, the maximum value of *D* parameter that the system can tolerate is 6.0. The velocity feedback coefficients are equivalent to the *D* module coefficients. The second order low-pass filters with a cut-of frequency 1kHz have been inserted into the system. The results indicate that all three control methods can stabilize the levitated rotor relatively rapidly. With PI+VF, the noise in the control current is significantly lower than the case with PID, resulting in a much quieter operation.

3.1. Experiments of vibration control by velocity feedback

The flexible rotor is driven by the motor at an acceleration of 180 r/min/s to the rated speed of 15,000 r/min. Three acceleration tests are performed using only PID (D=6.0) and PI+VF with coefficients of 6.0 and 9.0, respectively. It is important to note that since the rotor base is raised from the ground, the vibration of the rotor increases near 3,000-4,000 r/min and 10,000-11,000 r/min due to the base resonance. Taking the AMB-B as an example, the RMS values of vibration displacement are shown in Fig. 7.

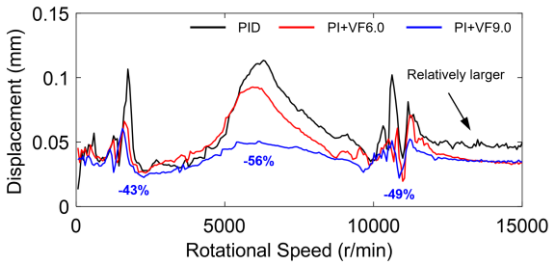

Fig. 7: Displacement response of AMB-B from 0 to 15,000 r/min.

From Fig. 7, the PI+VF control reduces the critical vibration of rigid modes by 43% compared to the PID controller. Higher resonance peaks appeared near the 1st bending mode critical speed. The vibration is slightly reduced under PI+VF6.0 control compared to PID, while the vibration is significantly reduced under PI+VF9.0 control by 56%. Sharp resonance peaks appear near the 2nd bending mode critical speed. The vibration at both ends is reduced by 49% under PI+VF9.0 control, which indicates that a larger velocity feedback coefficient increases the damping of the system significantly. When the rotational speed exceeds 12,000 r/min, the vibration displacement under PID control is relatively larger due to the increased contribution of noise to the RMS value of the displacement.

The control currents during the acceleration process are shown in Fig. 8. The comparison of the three curves shows that increasing the damping by a larger VF coefficient can suppress the resonances of the critical speeds without significantly increasing the current. The control currents are equal or even lower for the PI+VF control near the rigid modes, the 1st and the 2nd bending modes critical speeds, compared to the PID control alone.

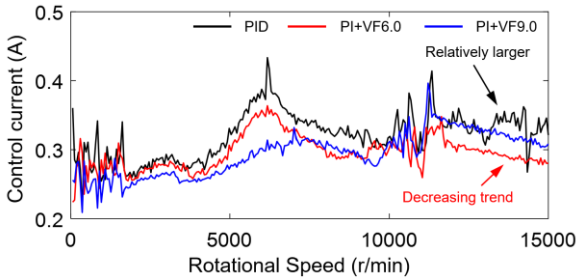

Fig. 8: Control currents of AMB-B from 0 to 15,000 r/min.

As the rotational speed exceeds 12,000 r/min, there is no obvious decreasing trend of the control current after passing the 2nd bending mode critical speed under PID control, since the sensor multiple frequencies and noise are further increased by the D blocks during the high-speed rotation. On the contrary, the currents of PI+VF have a significantly decreasing trend. The experimental results show that both the noise and vibration can be controlled at reasonable level by the integrated sensor and PI+VF control.

4. Conclusion

Aiming at the trade-off between the damping and noise of AMBs rotor systems, this paper proposed a novel integrated sensor which measuring vibration displacement and velocity in a single structure. On the basis of the inductive

displacement sensor, the vibration velocity is measured by obtaining the electromotive force generated by the change in air gap reluctance. The velocity measurement signal can be used to replace the differential blocks of conventional displacement based PID controller. Without increasing the noise level, the damping of the AMBs flexible rotor system can be significantly reduced, which yields notable improvements to the controller for the rotor system to pass its bending critical speeds. This research can be used in the AMBs rotor systems suffer from noise or operate over the critical speeds of bending modes.

References

[1] G. Schweitzer and E. H. Maslen, *Magnetic bearings: Theory, design, and application to rotating machinery.* New York, NY, USA: Springer, 2009.

[2] P. Berkelman and M. Dzadovsky, "Magnetic levitation overlarge translation and rotation ranges in all directions," *IEEE/AMSE Trans. on Mechatronics*, vol.18, no. 1, pp. 44-52, 2013.

[3] P. E. Allaire, D. W. Lewis, J. D. Knight, "Active vibration control of a single mass rotor on flexible supports," *Journal of the Franklin Institute*, vol. 315, no. 3, pp. 211-222, 1983.

[4] H. Fujiwara, K. Ebina, M. Ito, N. Takahashi, O. Matsushita, "Control of flexible rotors supported by active magnetic bearings," in *Proc. of the 8th International Symposium on Magnetic Bearings*, Mito, Japan. 2002: 145-150.

[5] F. Fernando, B. Enrique, "An ultrasonic ranging system for structural vibration measurements," *IEEE Transactions on Instrumentation and Measurement*, vol.40, no. 4, pp. 764-769, 1991.

[6] A. Sinharay, R. Rakshit and A. Khasnobish, "Single transducer sonar-radar for non-contact vibration detection," in *Proc. of 2019 IEEE SENSORS*, Montreal, QC, Canada, pp. 1–4, 2019.

[7] Y. Li, E. Dieussaert, R. Baets, "Miniaturization of laser doppler vibrometers—a review," *Sensors*, vol. 22, no. 13, pp.1-25, 2022.

[8] Lianhui Gao, *Magnetic circuits and ferromagnetic devices*. Beijing, China: Higher Education Press, 1982.